Combining nano-scale imprint lithography and reactive ion etching to fabricate high-quality surface relief gratings

Micha Haase[a,b], Nils Dittmar[a], Andrea Kneidinger[c], Patrick Schuster[c], Frederik Bachhuber[d], Christian Helke[a,b], and Danny Reuter[a,b]

[a]Fraunhofer ENAS, Technologie-Campus 3, 09126 Chemnitz, Germany
[b]University of Technology Chemnitz, Center for Microtechnologies, Reichenhainer Str. 70, 09126 Chemnitz, Germany
[c]EV Group (EVG), DI Erich Thallner Str. 1, 4782 St. Florian am Inn, Austria
[d]SCHOTT AG, Hattenbergstrasse 10, 55122 Mainz, Germany

ABSTRACT

In this study, we present a novel approach combining nano-scale imprint lithography (NIL) and reactive ion etching (RIE) to fabricate high-quality surface relief gratings (SRGs). This study provides valuable insights into the challenges and optimizations in fabricating SRGs from TiO_2 layers using the combination of NIL and RIE. The work was performed with SCHOTT RealView® substrates coated with a 100 nm TiO_2 layer and a NIL mask with pattern widths of 200 nm and a pitch of 400 nm. The substrates were processed using the SmartNIL® method to prepare the NIL mask. The advantage of removing the residual layer before the actual structuring of the TiO_2 using argon plasma was demonstrated in our research. This led to a significant increase in the selectivity between TiO_2 and the NIL resist UV/OA R18. Through the employment of a two-step etching process, which involved the removal of the residual layer with argon plasma and the use of a BCl_3-based reactive process with high ion energy, TiO_2 structures with a height of 100 nm and a sidewall angle of 75° were successfully created. An effective selectivity of 0.84 was achieved for this two-step process.

Keywords: nano-scale imprint lithography, reactive ion etching, surface relief gratings, titanium dioxide

1. INTRODUCTION

Among the various waveguide technologies, coupling and decoupling of light using surface relief gratings (SRGs) has become a commonly used method.[1] Two methods on wafer-level are usually used to fabricate SRGs: First, additive e.g. via nanoimprint lithography into a resin[2] and second subtractive e.g. via etching into the waveguide material[3,4] or an additional (inorganic) layer.[5]

In the fabrication of optical grating structures based on additive methods, especially when using titanium dioxide (TiO_2) and E-beam technology, complex procedures are sometimes required. Quan et al.[4] reported the fabrication of TiO_2 grating structures using a chrome hard mask and subsequent transfer through reactive ion etching (RIE), with the chrome patterning achieved through lift off. On the other hand, Liu et al.[3] used RIE for structuring the metal hard mask, which was then used for patterning TiO_2. In the studi of Hashemi et al.,[6] a very complex technology sequence was described, where a dual-resist system enabled the lift-off of nickel. This only refers to the upper part of the two-component hard mask system consisting of nickel Ni and silicon dioxide (SiO_2). Reactive ion etching was then used to etch TiO_2 through this hard mask system. These studies highlight the complexity of established subtractive methods for the fabrication of TiO_2-SRGs, which motivates the investigation of the feasibility of combining nano-scale imprint lithography (NIL) and RIE, particularly for this material.

The interest in TiO_2 is based on its properties. It exhibits very low losses and is capable of achieving high diffraction efficiencies and high extinction ratios, why it is sometimes described as a nearly loss-less dielectric.[7]

Further author information: (Send correspondence to Micha Haase)
Micha Haase: E-mail: micha.haase@enas.fraunhofer.de, Telephone: 0049 371 45001 497
B.B.A.: E-mail: bba@cmp.com, Telephone: +33 (0)1 98 76 54 32

Advanced Fabrication Technologies for Micro/Nano Optics and Photonics XVII, edited by Georg von Freymann, Eva Blasco, Debashis Chanda, Proc. of SPIE Vol. 12898, 128980L · © 2024 SPIE · 0277-786X · doi: 10.1117/12.3002254

The high refractive index of TiO_2 is of particular interest. Although there are methods to increase the refractive index of materials through doping,[3] the authors in this explain that there is currently no material that can replace the role of TiO_2 in the visible wavelength range. Due to the outstanding properties of TiO_2, the processing of this material is of great importance. In order to enable its use in various applications, wafer-level process sequences and integration concepts need to be developed. These technologies are important for maximizing the functionality and performance of TiO_2 in various applications.

Although some scientific papers have demonstrated the potential of NIL for optical applications very well,[8–10] our literature research indicates that the application of nanoimprint lithography for the fabrication of SRGs using TiO_2 has been relatively underrepresented. For this reason, we investigated the fabrication process of SRGs using TiO_2. The main focus of our investigation was on the transfer of the structure into TiO_2 through the use of NIL resist. In this study, we demonstrate that the formal application of fluorocarbon-based RIE processes with a NIL resist mask is not feasible. Furthermore, we show that the utilization of BCl_3-based processes can be utilized for structure transfer in principle, but the quality of the etched sample is significantly reduced due to the formation of etch residues. We found that the opening process of the residual layer plays a crucial role in patterning, and we show that the break-through of the residual layers with an argon plasma can have significant effects on the selectivity between TiO_2 and NIL resist.

2. METHODS AND MATERIALS

2.1 Substrate preparation

To investigate the structuring of TiO_2, this study utilized SCHOTT RealView® substrates coated with a 100 nm thick layer of TiO_2. SCHOTT RealView® is available in a broad variety of refractive indices from 1.5 to more than 2.0 and all glass types are compatible with TiO2 coatings with a thickness of >30 nm.[11] To create the desired structures, a total of 16 imprints were applied to the substrates, with a height of approximately 180 nm, a width of 200 nm and a pitch of 400 nm. The SmartNIL® process was employed, which procedure is illustrated in Figure 1. In general, this technology (developed by EVG) consists of two main steps - the

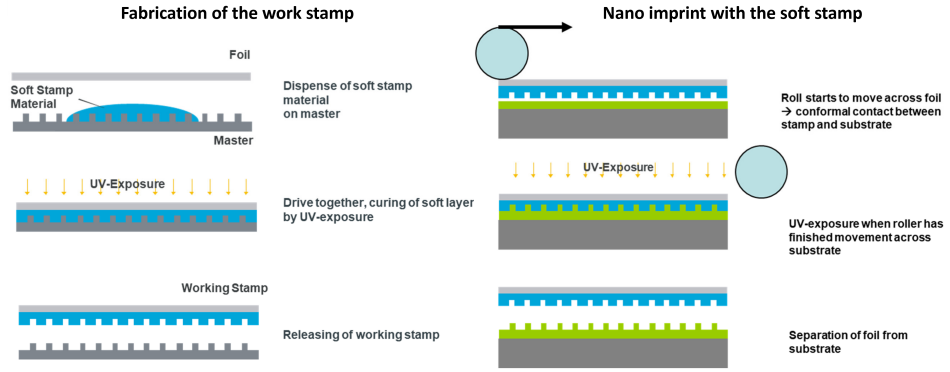

Figure 1. Schematic representation of the SmartNIL® process flow developed by EVG

replication of the working stamp (left in Figure 1) and the imprint process performed with the working stamp (right in Figure 1). The advantage of this approach is that the master stamp is never directly used for the imprint, and the soft stamp can have specific key properties such as anti-adhesive characteristics. The fabrication of the working stamp begins by applying the soft stamp material onto the master, as depicted in Figure 2. Subsequently, a UV-transparent foil is pressed onto the coated master, and under pressure and UV irradiation, the pattern of the master stamp is transferred onto the soft material. Then, the foil, along with the structured soft material, is removed from the master, completing the fabrication of the working stamp or soft stamp for the actual imprint process. Essentially, a transparent soft stamp is created for the transfer process into the NIL resist. For the imprint process using transparent soft stamps, the SCHOTT RealView® substrates were coated with a NIL resist. The organic UV/OA R18 resin was applied to the substrates using spin coating,

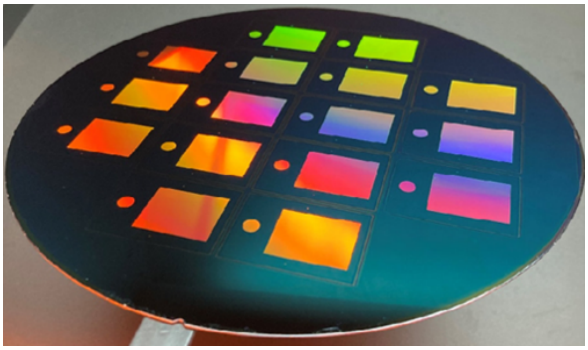

Figure 2. Photo of the used master, showing the 16 individually SRGs with in- and outcoulpling strucutres

utilizing the EVG®101 300 mm Advanced Spin Coating System. All imprint processes were performed using the EVG®7200 automated UV Nanoimprint System (an imprint example is shown in Figure 3).

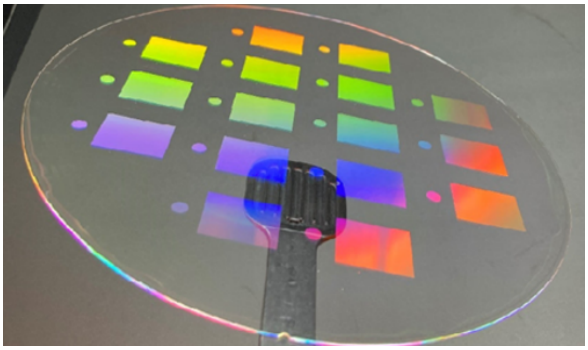

Figure 3. Photo of the SCHOTT RealView® substrate with the NIL resist mask

Analyses with an AFM of these fabricated structures revealed that the height of the grating structures varies between 177 nm and 183 nm at all measured positions (see Figure 4). Comparisons with AFM measurements on the master stamp showed good agreement between the heights and widths of the structures on the coated glass substrates and the master stamp. Therefore, we assume that a good transfer of the structure has occurred.

To determine the residual layer thickness (RLT), test imprints were performed on standard Si wafers. To measure the RLT, scratches were introduced into the structures, resulting in an RLT of 18 nm. It is reasonable

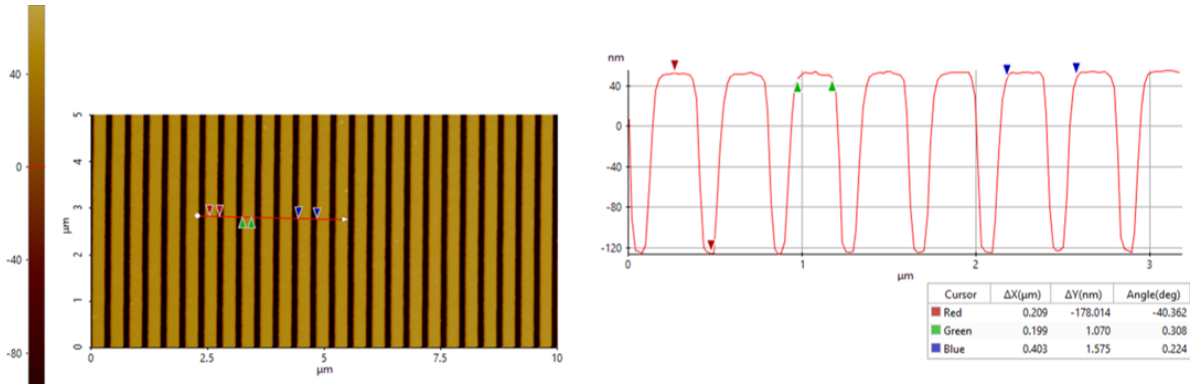

Figure 4. AFM measurement of a grating; height: 178 nm, width: 199 nm, pitch: 403 nm

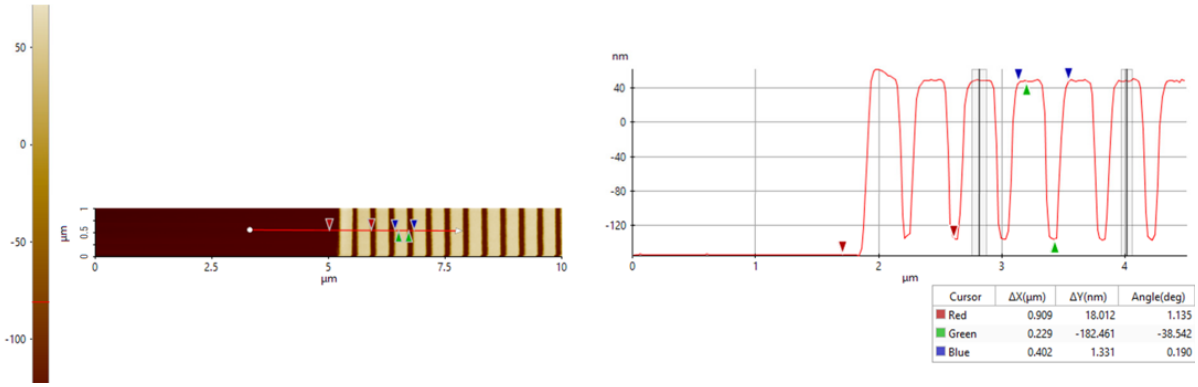

Figure 5. AFM measurement over a scratch on a test imprint on a grating to determine RLT: 18 nm , structure height: 182 nm, pitch: 402 nm

to assume that the RLT on the glass substrates is similar, as both the height and pitch are in the same order of magnitude as observed on the TiO_2 coated glass substrates (see Figure 5).

2.2 Reactive ion etching

All etching processes in this study were carried out on the Applied Materials Centura 5200 cluster tool. The tool is a multi-chamber system designed for 200 mm wafers, with its process chambers used for etching various materials under different conditions. The system has two different etching chambers, referred to by the manufacturer as DPS (decoupled plasma source) and eMxP+. Both chambers of the system were utilized in this study.

The concept of the eMxP+ etching chamber is based on a capacitively coupled RIE process chamber, with pairs of magnets arranged perpendicularly around the chamber body. By varying currents through these magnets, a rotating magnetic field is generated around the process chamber, leading to an increase in the ionization rate in the plasma region and an enhanced etching rate at low process pressures below 200 mTorr. For this study, the process pressure was fixed at 100 mTorr, while the magnetic field was kept at 20 Gauss and the RF power at 600 W. Processes with gases CF_4 and CHF_3 were investigated, whereby the gas mixture was varied. In other words, the fluorine-to-carbon ratio of the process was changed to examine the influence of polymerization on the substrate.

The DPS chamber is based on the concept of ICP (inductively coupled plasma), where two sources couple RF power, one inductively and the other capacitively, into the reactor chamber. Similar to systems with capacitively coupled plasma, the electrode holding the wafer receives a negative potential when RF power is applied. The second plasma source allows power to be fed through an antenna wrapped around the dome (a bowl-shaped cover separating the process chamber from the atmosphere). The inductive power coupling results in increased ion and radical density in the plasma space. The power coupling is done separately, which allows the separate control of radical density and ion bombardment. In this study, we investigated the structuring process of TiO_2 in the DPS chamber using BCl_3 chemistry. We also considered the effect of gas additives Ar and CH_4. For resist masks produced using NIL, it is necessary to perform a so-called break-through step prior to the actual structuring. The need of this step is demonstrated in section 3. Therefore, break-through processes using Ar and the etching gas itself were investigated in the DPS chamber, too. The substrate analysis after the structuring processes was carried out using scanning electron microscopy (SEM) and focused ion beam (FIB). Initial analyses resulted in significant overexposure artifacts due to the highly insulating nature of the examined substrates. To mitigate electron beam-induced charging effects, particularly for FIB analyses, the substrates were coated after plasma structuring with a thin layer of aluminum approximately 3 to 5 nm thick.

3. RESULTS

Figure 6 shows results when various patterning processes are directly applied to the substrates with an imprint mask. The processes shown are based on fluorine chemistry using gases CF_4 and CHF_3 in a 1:1 ratio (Fig. 6a)),

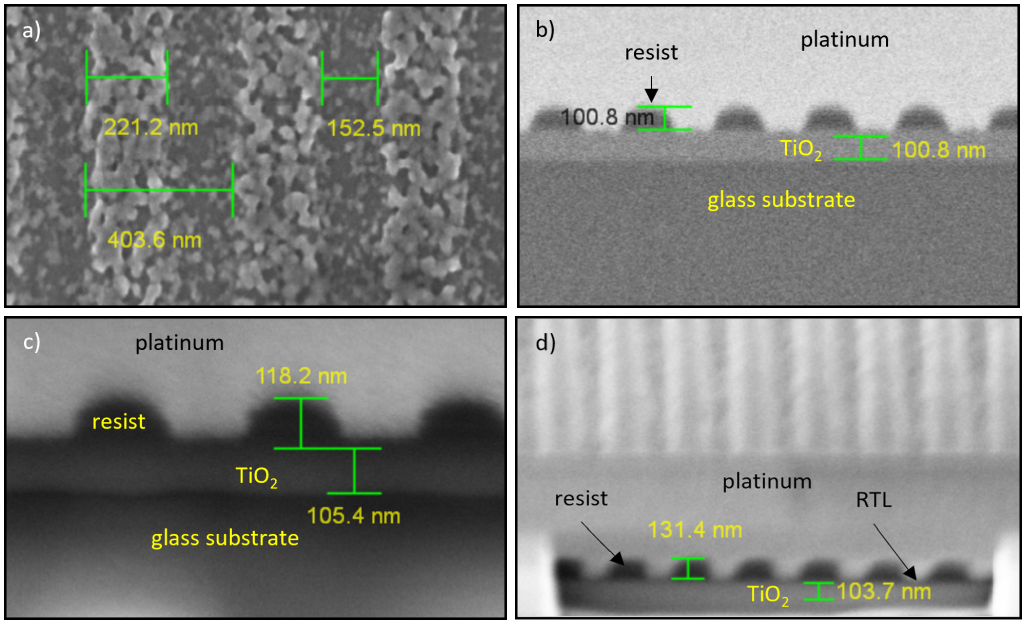

Figure 6. SEM images after processing in different etching plasmas: a) gas mixture of CF_4 and CHF_3; b) and c) BCl_3 and Ar at different process times; d) BCl_3/Ar gas mixture with the addition of CH_4.

as well as three BCl_3-based processes with the addition of Ar (Fig. 6b) and 6c)) and CH_4 (Fig. 6d)). While cross-sectional images could be obtained through FIB for the samples etched in the DPS chamber, this was not possible for the sample treated with CF-based chemistry, despite the aluminum coating. Only surface images of this sample could be taken.

In the surface SEM image (Fig. 6a)), it is evident that the thin aluminum layer, deposited using physical vapor deposition, is not fully closed. This phenomenon is attributed to strong polymerization during the plasma etching process. It can be concluded that under the given process conditions in the MERIE chamber, there was no etching but rather polymer deposition. This hypothesis is supported by the alteration in the width of the trenches and ridges. Although the pitch is still measured with 403 nm, there is an increase in ridge width accompanied by a narrowing of the trenches. This phenomenon can only be explained by deposition, i.e. polymerization, occurring on the NIL resist surface.

The substrates for the SEM images of Fig. 6b) and Fig. 6c) were processed under identical process conditions. The only difference between these process parameters was the process time, which was 70 s (Fig. 6b)) and 110 s (Fig. 6c)). The ICP power, bias power, pressure, and gas mixture ratio of BCl_3 and Ar were kept constant at 900 W, 100 W, 5 mTorr, and 1:1, respectively. Additionally, the substrate for Figure 6d) was treated similarly to the substrate for Figure 6b), with the addition of CH_4 during the process.

In the images of Figure 6b), c) and d), the interface between the glass substrate and TiO_2 is clearly visible. The thickness of the TiO_2 layer was determined to be approximately 100 nm in all three images. Since this thickness corresponds to the initial layer thickness, it is evident that no etching of the TiO_2 layer occurred in any of the cases. This can be attributed to the presence of a residual layer at the bottom of the trenches in each case. Additionally, it is observed that in Figure 6b) and c), the vertical removal of the NIL resist is on the order of 80 nm (initial thickness approximately 180 nm, see section 2), while in Figure 6d), it is slightly less, around 50 nm. The reduced removal in this process is attributed to the addition of CH_4, which increases polymerization on the resist surface and consequently decreases the resist etch rate. Furthermore, in Figure 6c) and d), the situation is such that the residual layer is still detectable even by SEM imaging. This leads to the conclusion that the residual layer evidently exhibits a higher resistance to plasma chemistry and ion bombardment compared to the actual NIL mask.

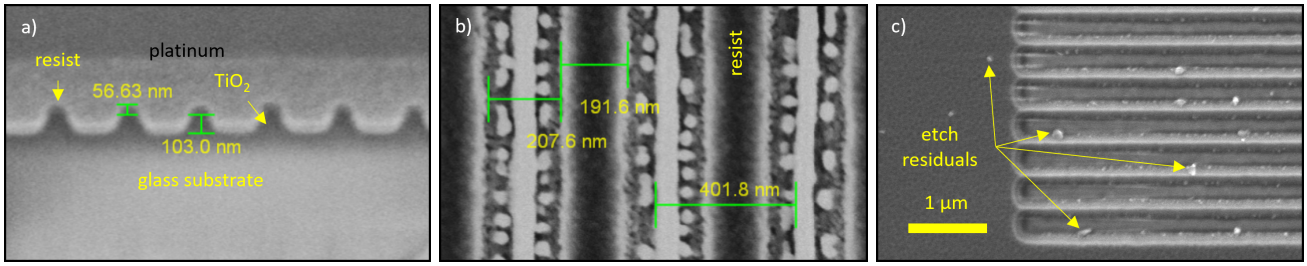

Figure 7. a) Structuring of TiO_2 with a preceding BCl_3-based break-through process. b) Etch residue observed immediately after a break-through process using BCl_3. c) Etch residue observed after a two-step TiO_2 etching process and long over etching

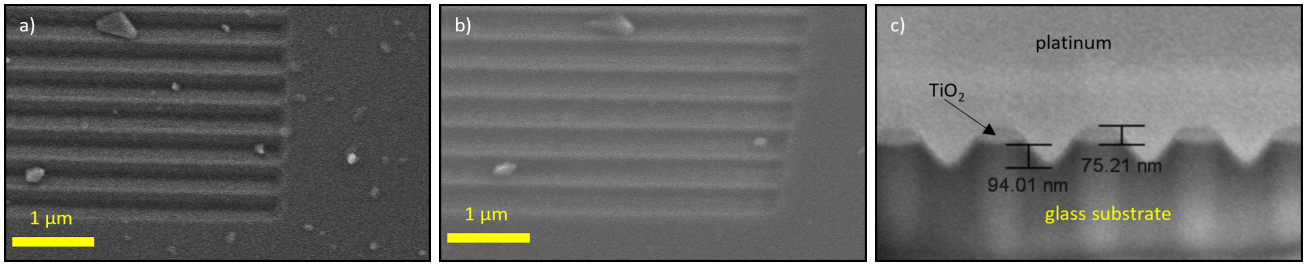

Figure 8. Removal of the residuals: a) after a BCl_3-based plasma treatment, b) after subsequent argon removal. However, at the expense of structural quality including resist removal and sputtering attack of the glass substrat.

Now, in Figure 6b), the residual layer is not visible, suggesting that the process conditions enable the utilization as a breakthrough process for the residual layer, allowing for the implementation of a two-step etching process for reactive etching of TiO_2. Results for this approach are shown in Figure 7. Figure 7a) depicts structured TiO_2 lines obtained using a BCl_3-based break-through process with the following parameters: 900 W ICP power, 100 W bias power, 5 mTorr process pressure, and a gas mixture of BCl_3 and Ar in a 1:1 ratio. Subsequently, TiO_2 etching was performed using the following parameters: 600 W ICP power, 300 W bias power, 5 mTorr process pressure, and a gas mixture of BCl_3 and Ar in a 1:3 ratio. In the SEM image, it is challenging to recognize the interface between the glass and TiO_2, as well as between TiO_2 and the resist. Therefore, the exact measurement of the remaining resist on the TiO_2 cannot be precisely determined. The presence of remaining resist can be concluded from the fact that the total height of a line, approximately 160 nm, is greater than the deposited TiO_2 layer thickness of 100 nm. However, during the investigation, it was observed that this two-step process tends to result in residue formation, which occurs even after opening the residual layer (see Fig. 7b)). Furthermore, even with complete consumption during excessive over-etching of the substrate, residue can still remain. We attribute these etch residues to non-volatile $TiCl_x$ compounds, some of which exhibit high boiling temperatures.[12]

In the scope of this study, we have established that we can decrease these residuals by employing a straightforward Ar plasma treatment, or more precisely, by employing inert ion bombardment for their removal. This indicated by Figure 8. The figure shows two surface images (a)) and (b)) as well as a cross-sectional image (c)) obtained using FIB. While Figure 8a) displays the residuals after a BCl_3 process, Figure 8b) demonstrates that they can be reduced through an Ar plasma treatment. However, the cross-sectional view of the sample shows that this process is at the cost of structural quality, leads to a loss of resist material and an sputtering attack of the glass substrate.

One possible strategy is to remove the residues that have formed due to BCl_3 break-through before the actual TiO_2 structuring using an Ar plasma. The result of this approach is summarized in Figure 9. The figure illustrates a three-step sequence for structuring. The first step involves a BCl_3-based break-through (Fig. 9a), followed by the reduction of residues in an Ar plasma (Fig. 9b), and finally, the actual structuring with increased ion bombardment in a BCl_3/Ar ratio of 1:3 (Fig. 9c). These images were taken on the same sample to analyze

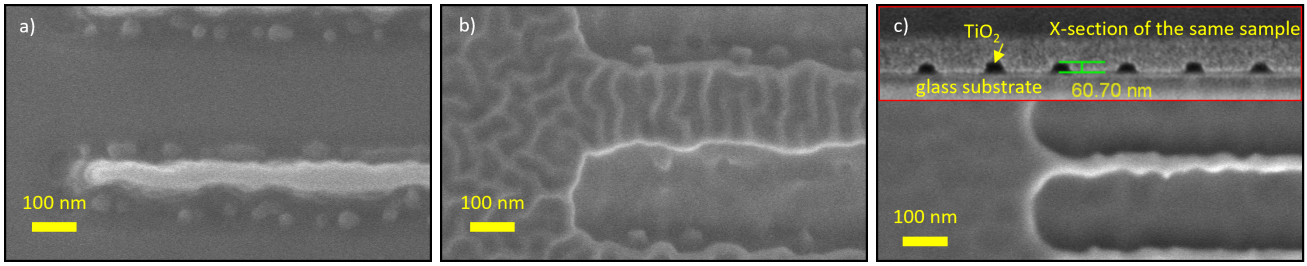

Figure 9. Combined process sequence: a) BCl_3-based break-through (900 W ICP power, 100 W bias power 1:1 BCl_3/Ar mixture); b) Ar plasma resudual removal (100 W bias power); TiO_2-etching (600 W ICP power, 300 W bias power, 1:3 BCL_3/Ar gas mixture - each single step at 5 mTorr

the condition after each step. Residues are clearly visible after the BCl_3-based break-through, particularly at the areas of structural changes. The use of Ar with exclusive bias power reduces the number of residues, as expected. Interestingly, the Ar-plasma treatment causes a surface modification of the NIL resist. This is interpreted as a form of resist cross-linking induced by the vacuum ultraviolet (VUV) radiation emitted by excited argon ions. The strong VUV intensity of argon is well-known from studies on damage analysis of dielectric materials,[13,14] supporting this assumption. According to the results shown in Fig. 6a), approximately 30 nm (estimated NIL etch rate of 1.2 $\frac{\text{nm}}{\text{s}}$) of TiO_2 remained available for structuring in the specific case after the BCl_3-based break-through process. Assuming an etch rate of 0.8 $\frac{\text{nm}}{\text{s}}$ for TiO_2 (see Fig. 7), the TiO_2 should have been completely etched away after an etching time of 210 s, as the resist should have been consumed after approximately 25 s, and within the remaining 185 s, a total layer thickness of approximately 150 nm would have been etched. Actually, the TiO_2 is not completely removed, as evident from both surface and cross-sectional images of this sample (see Fig. 9a). Although complete resist consumption is observed, TiO_2 structures with a height of 61 nm are still present. Furthermore, the surface shows no etch residues. The observed phenomenon indicates that the cross-linking of the resist plays a role in improving selectivity by densifying the NIL resist, while simultaneously the residual layer during this densification process could be removed. Despite the cross-linking, a physical removal of the NIL resist can still be expected due to ion bombardment. Therefore, the results of Fig. 9 suggest that a break-through in Ar is the most appropriate approach. During the removal of the residual layers, the resist is already being cross-linked, resulting in a thicker resist layer that can then be utilized for the etching of TiO_2.

Indeed, this phenomenon was also observed in our experiments, if Figure 10 is considered. The effect of cross-linking (a) is clearly evident after applying a 150 s long Ar plasma. The successful removal of the residual layer is indicated by the absence of any cross-linked resist structures on the bottom of the trench. In our investigations, we were able to demonstrate that these cross-linked resist structures are present on the trench bottom if the break-through process is not successful.

Considering the patterning result after applying an etching process with higher ion energy (Fig. 10b)), it is seen that no etch residuals can be found on the resist surface and trench bottom, respectively. The cross-sectional analysis reveals 100 nm high TiO_2 lines with a residual resist thickness of 56 nm on top. While the interface between the resist and TiO_2 is challenging to distinguish, the overall height of 156 nm probably consists of both the residual resist and the TiO_2. Two reasons support this statement: First, the initial layer thickness of the TiO_2 was 100 nm. Secondly, an over-etch of the sample into the glass substrate can be excluded based on the experiment in which intentional over-etching was performed, resulting in an extreme taper profile in the glass (vgl. Fig 9c)). Contrarily, a very smooth trench bottom is observed here, indicating that the process for structuring TiO_2 exhibits good selectivity relative to the glass substrate used in this study. The process sequence shows in Figure 9 presents a possible approach for the reactive structuring of TiO_2 using NIL resist. Currently, an effective selectivity of 0.84 can be achieved, and the analysis of line widths leads to a flank angle of 75°.

4. DISCUSSION

In contrast to other studies where TiO_2 SRGs were fabricated using hard masks, this study investigates the structure transfer using NIL resist. While Lee et al. and Hashemi et al. demonstrate the application of fluorine-

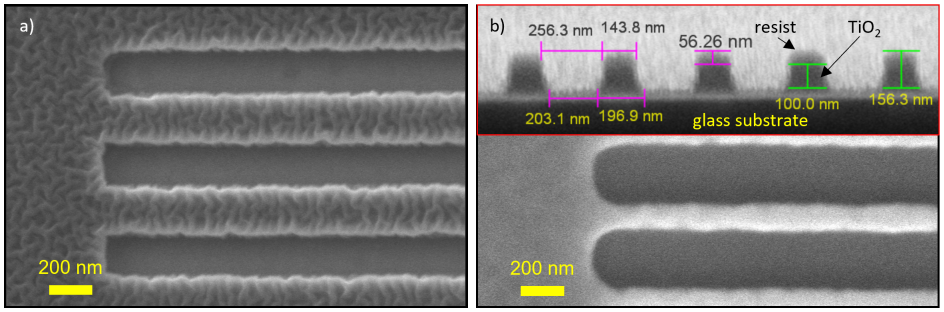

Figure 10. Tow-step TiO_2 patterning: a) Top view after residual layer breakthrough performed in a Ar plasma for 150 s; b) Top view and cross section after etching of TiO_2 using a BCl_3/Ar gas mixture of 1:3, 600 W ICP power, 300 W bias power, and 5 mTorr

based chemistry through a single-step reactive ion etching process for TiO_2 structuring in their studies,[6,7] our experiments show that this is not feasible in the case of using NIL resist because of the presence of the residual layer. It should be noted that in the mentioned studies an ICP reactor was used for the structuring, while our investigation was performed in a MERIE chamber. However, it should be informed to the reader that structuring of TiO_2 in the MERIE chamber after the argon break-through process has also been achieved successfully. Unfortunately, these investigations could not be completed at the time of writing this report.

For sure, it is no innovation to remove the residual layer. Typically, oxygen plasmas are used to open the residual layers.[8,9] However, it is known that removing the residual layer with O_2 RIE reduces the line width and increases the trench width. Yang et al. explain that the imprinted patterns can be degraded during the residual layer removal process by oxygen plasma etching. In contrast, Uehara et al. have shown that anisotropic etching in a pure oxygen atmosphere is possible when process conditions with low gas residence time and increased mean free path are ensured, which qualitatively means working with low process pressure and high gas flow. Based on our current results, we still recommend using Ar for the removal of the residual layers. Firstly, we expect that the observed cross-linking behavior of the NIL resist will be less pronounced, as O_2 has fewer emission lines in the VUV range compared to Argon.[15,16] Secondly, we expect that the chemical resist removal will increase in the presence of oxygen radicals. The feasibility of using a continuous directional sputter-etch process using a low-pressure Ar plasma for the removal of the residual layers has also been demonstrated by Dirdal et al. in the structuring of silicon via NIL.[10] However, in contrast to our study, they do not address the resist modification and do not report on structural modifications of the resist caused by the Ar breakthrough.

Although Tonotani et al. demonstrate that the etching rate of TiO_2 in Cl_2 plasma is significantly higher than in polymerizing plasmas such as BCL_3 and CHF_3,[17] we further recommend, especially for optical applications with glass substrates, to continue using BCl_3. The reason for this is that glass is very similar to SiO_2 and the knowledge that a high selectivity towards SiO_2 can be achieved.[18] In fluorine-based plasmas, on the other hand, the expectation of achieving comparable selectivity is not high. However, it is not expected that infinite selectivity towards the substrate can be achieved. Because, as reported by Joo et al.,[19] it was observed in our study that etching residues can only be prevented under increased ion bombardment.

5. CONCLUSION

In this study, the feasibility of fabricating TiO_2 surface relief gratings on SCHOTT RealView® substrates was investigated using a combination of EVG®'s SmartNIL® technology and reactive ion etching. It was established that a two-step etching process consisting of residual layer removal with argon plasma and a BCl_3-based reactive process with high ion energy can be utilized for etching TiO_2. Using this approach, we were able to create TiO_2 structures with a height of 100 nm and a sidewall angle of 75°, with an effective selectivity of 0.84 for this two-step process.

For further studies, the effect of chamber conditioning needs to be investigated. During the study, difficulties in reproducibility were observed, and particles were found on the wafers even after simple argon plasma treatments,

which, based on current knowledge, can only be attributed to redeposition of etch residues from the chamber walls. Therefore, the need of chamber cleaning after TiO_2 etching cannot be ruled out at this point. Furthermore, it remains to be seen if the fluorine-based structuring will be successful after achieving successful break-through, which should be explored in future studies. In order to complete the fabrication of SRGs, additional efforts on developing effective resist removal procedures are necessary.

REFERENCES

[1] Ding, Y., Yang, Q., Li, Y., Yang, Z., Wang, Z., Liang, H., and Wu, S.-T., "Waveguide-based augmented reality displays: perspectives and challenges," *eLight* **3**, 24 (12 2023).

[2] Thanner, C., Dudus, A., Treiblmayr, D., Berger, G., Chouiki, M., Martens, S., Jurisch, M., Harbaum, J., and Eibelhuber, M., "Nanoimprint lithography for augmented reality waveguide manufacturing," *Optical Architectures for Displays and Sensing in Augmented, Virtual, and Mixed Reality (AR, VR, MR)* , 34, SPIE (2 2020).

[3] Liu, Y., Qu, G., Jiang, X., Han, J., Ji, Z., Liu, Z., Song, Q., Yu, S., and Xiao, S., "Slanted tio_2 metagratings for large-angle, high-efficiency anomalous refraction in the visible," *Laser and Photonics Reviews* **17** (6 2023).

[4] Quan, D., Jia, H., Li, W., Cheng, X., and Kwok, H. S., "Large form birefringence realized by dielectric subwavelength grating," *Digest of Technical Papers - SID International Symposium* **50**, 1110–1113, Blackwell Publishing Ltd (2019).

[5] Helke, C., Reinhardt, M., Arnold, M., Schwenzer, F., Haase, M., Wachs, M., Goßler, C., Götz, J., Keppeler, D., Wolf, B., Schaeper, J., Salditt, T., Moser, T., Schwarz, U. T., and Reuter, D., "On the fabrication and characterization of polymer-based waveguide probes for use in future optical cochlear implants," *Materials* **16**(1) (2023).

[6] Hashemi, E., Bengtsson, J., Gustavsson, J. S., Carlsson, S., Rossbach, G., and Åsa Haglund, "Tio_2 membrane high-contrast grating reflectors for vertical-cavity light-emitters in the visible wavelength regime," *Journal of Vacuum Science & Technology B, Nanotechnology and Microelectronics: Materials, Processing, Measurement, and Phenomena* **33** (9 2015).

[7] Lee, K. J., Giese, J., Ajayi, L., Magnusson, R., and Johnson, E., "Resonant grating polarizers made with silicon nitride, titanium dioxide, and silicon: Design, fabrication, and characterization," *Opt. Express* **22**, 9271–9281 (Apr 2014).

[8] Ahn, S.-W., Lee, K.-D., Kim, J.-S., Kim, S. H., Lee, S. H., Park, J.-D., and Yoon, P.-W., "Fabrication of subwavelength aluminum wire grating using nanoimprint lithography and reactive ion etching," *Microelectronic Engineering* **78-79**, 314–318 (2005). Proceedings of the 30th International Conference on Micro- and Nano-Engineering.

[9] Yang, K.-Y., Kim, J.-W., Hong, S.-H., Hwang, J.-Y., and Lee, H., "Fabrication of nano-scale phase change materials using nanoimprint lithography and reactive ion etching process," *Thin Solid Films* **518**(20), 5662–5665 (2010). Special Section: Materials Today Asia Conference.

[10] Dirdal, C. A., Milenko, K., Summanwar, A., Dullo, F. T., Thrane, P. C. V., Rasoga, O., Avram, A. M., Dinescu, A., and Baracu, A. M., "Uv-nanoimprint and deep reactive ion etching of high efficiency silicon metalenses: High throughput at low cost with excellent resolution and repeatability," *Nanomaterials* **13**(3) (2023).

[11] Sprengard, R., "Optical components for waveguides: progress in high refractive index glass wafers for diffractives architectures and manufacturing aspects of reflective waveguides ," in [*SPIE AR, VR, MR Industry Talks 2023*], Kress, B. C. and Peroz, C., eds., **12450**, 124500X, International Society for Optics and Photonics, SPIE (2023).

[12] Norasetthekul, S., Park, P., Baik, K., Lee, K., Shin, J., Jeong, B., Shishodia, V., Lambers, E., Norton, D., and Pearton, S., "Dry etch chemistries for TiO_2 thin films," *Applied Surface Science* **185**, 27–33 (12 2001).

[13] Zotovich, A., Proshina, O., Otell, Z. E., Lopaev, D., Rakhimova, T., Rakhimov, A., Marneffe, J. F. D., and Baklanov, M. R., "Comparison of vacuum ultra-violet emission of Ar/CF_4 and Ar/CF_3I capacitively coupled plasmas," *Plasma Sources Science and Technology* **25** (2016).

[14] Proshina, O. V., Rakhimova, T. V., Zotovich, A. I., Lopaev, D. V., Zyryanov, S. M., and Rakhimov, A. T., "Multifold study of volume plasma chemistry in Ar/CF_4 and Ar/CHF_3 ccp discharges," *Plasma Sources Science and Technology* **26** (2017).

[15] Lee, J. and Graves, D. B., "The effect of vuv radiation from Ar/O_2 plasmas on low-k sioch films," *Journal of Physics D: Applied Physics* **44**, 325203 (jul 2011).

[16] Jaritz, M., Behm, H., Hopmann, C., Kirchheim, D., Mitschker, F., Awakowicz, P., and Dahlmann, R., "The effect of uv radiation from oxygen and argon plasma on the adhesion of organosilicon coatings on polypropylene," *Journal of Physics D: Applied Physics* **50**, 015201 (1 2017).

[17] Tonotani, J., Iwamoto, T., Sato, F., Hattori, K., Ohmi, S., and Iwai, H., "Dry etching characteristics of tin film using Ar/CHF_3, Ar/Cl_2, and Ar/BCl_3 gas chemistries in an inductively coupled plasma," *Journal of Vacuum Science & Technology B: Microelectronics and Nanometer Structures Processing, Measurement, and Phenomena* **21**, 2163–2168 (9 2003).

[18] Sungauer, E., Mellhaoui, X., Pargon, E., and Joubert, O., "Plasma etching of hfo2 in metal gate cmos devices," *Microelectronic Engineering* **86**, 965–967 (2009).

[19] Joo, Y.-H., Woo, J.-C., and Kim, C.-I., "Dry etching properties of TiO_2 thin film using inductively coupled plasma for resistive random access memory application," *Transactions on Electrical and Electronic Materials* **13**, 144–148 (6 2012).